# Thermosensitive TRP channel pore turret is part of the temperature activation pathway

Fan Yang[a], Yuanyuan Cui[a,b], KeWei Wang[b], and Jie Zheng[a,1]

[a]Department of Physiology and Membrane Biology, University of California Davis, Davis, CA 95616; and [b]Department of Neurobiology, Neuroscience Research Institute, Peking University Health Science Center, Beijing 100083, China

Edited* by Richard Warren Aldrich, University of Texas, Austin, TX, and approved March 9, 2010 (received for review January 11, 2010)

**Temperature sensing is crucial for homeotherms, including human beings, to maintain a stable body core temperature and respond to the ambient environment. A group of exquisitely temperature-sensitive transient receptor potential channels, termed thermoTRPs, serve as cellular temperature sensors. How thermoTRPs convert thermal energy (heat) into protein conformational changes leading to channel opening remains unknown. Here we demonstrate that the pathway for temperature-dependent activation is distinct from those for ligand- and voltage-dependent activation and involves the pore turret. We found that mutant channels with an artificial pore turret sequence lose temperature sensitivity but maintain normal ligand responses. Using site-directed fluorescence recordings we observed that temperature change induces a significant rearrangement of TRPV1 pore turret that is coupled to channel opening. This movement is specifically associated to temperature-dependent activation and is not observed during ligand- and voltage-dependent channel activation. These observations suggest that the turret is part of the temperature-sensing apparatus in thermoTRP channels, and its conformational change may give rise to the large entropy that defines high temperature sensitivity.**

conformational change | fluorescence resonance energy transfer | temperature sensing | thermodynamics

Temperature-sensitive transient receptor potential channels, or thermoTRPs, include four heat-activated channels (TRPV1–4) and two cold-activated channels (TRPM8 and TRPA1) that exhibit nicely spaced activation temperatures covering the physiological temperature range (1–4). These are expressed in dorsal root ganglion sensory neurons, keratinocytes, and other cells (1). Temperature changes cause rapid, reversible activation of thermoTRP channels in both native cells (3) and expression systems (Fig. 1 *A* and *B*). Depolarizing currents through these nonselective, cation-permeable channels lead to the generation of action potentials (5) or the release of messenger molecules (6, 7) that encodes temperature information. Structurally, thermoTRPs resemble voltage-dependent potassium channels, with four subunits surrounding a central ion permeation pore (4). Each subunit contains six transmembrane segments (S1–S6) and long intracellular N and C termini. The channel pore is formed by S6 and a P-loop that in most thermoTRPs is noticeably longer than those of KcsA and voltage-gated potassium channels (8, 9). Unique TRP channel structural elements, such as TRP Box immediately after S6 and N-terminal ankyrin repeats, are found in most thermoTRPs.

Despite extensive research, the channel structure bestowing high temperature sensitivity on thermoTRPs remains elusive. ThermoTRP channels are polymodal sensors responsive to a wide range of physical and chemical stimuli, such as transmembrane voltage, ligands, and pH. It has been proposed that heat might control thermoTRP activation by shifting the channel's response to these stimuli (10, 11). Alternatively, synergistic activation by multiple stimuli may arise from allosteric coupling among different channel structures (12). In the present study, we find that the temperature activation pathway is distinct from ligand and voltage activation pathways. In addition, based on thermodynamic, functional, and structural evidence, we propose that the pore turret is an important part of the heat activation machinery.

## Results

**Thermodynamic Characterization of ThermoTRP Channels.** Thermodynamic law dictates that a highly temperature-sensitive process originates from a large entropic change ($\Delta S$). This can be seen in the Gibbs free energy equation, $\Delta G = \Delta H - T\Delta S$, in which the free energy ($\Delta G$) for a reversible reaction is linearly dependent on temperature ($T$) with a slope factor ($\Delta S$). To better understand the molecular mechanism underlying heat-induced thermoTRP activation, we quantified entropic and enthalpic ($\Delta H$) changes from temperature-induced open probability changes recorded in inside-out patches formed from HEK293 cells expressing each thermoTRP channel type (Fig. 1 *C* and *D*).

As expected, heat-induced activation of TRPV1–4 channels exhibited a large positive entropic change of 100–300 cal/mol/K (Fig. 1*E*), causing a steep decrease in $\Delta G$ in response to temperature increases. Conversely, activation of the cold-sensitive TRPM8 channel exhibited a large negative $\Delta S$ of −200 cal/mol/K, which led to a steep decrease in $\Delta G$ in response to temperature drops. (Under our experimental conditions using cell-free patches and $Ca^{2+}$-free solutions, TRPA1 did not yield any temperature-dependent current even when the temperature dropped below 10 °C.) Thermodynamic analysis also revealed a large positive $\Delta H$ of 30–80 kcal/mol for TRPV1–4 and a large negative $\Delta H$ of −60 kcal/mol for TRPM8. The magnitude of these values is better appreciated in comparison with the $\Delta S$ and $\Delta H$ for oxygen binding to hemoglobin, which are −30 cal/mol/K and −10 kcal/mol, respectively (13). The large $\Delta S$ and $\Delta H$ values, consistent with previous reports of individual thermoTRP channels (see, e.g., refs. 10 and 14), are similar to those seen in CLC-0 chloride channels. CLC-0 has two distinct gating modes, an extremely temperature-sensitive common gating and a "normal" fast gating (15). Indeed, both $\Delta S$ and $\Delta H$ are about 10-fold larger for common gating compared with those for fast gating (Fig. 1*E*).

Quantification of the thermodynamic parameters illustrates how thermoTRPs operate as biological thermosensors. With a large change in the "orderness" ($\Delta S$), likely through conformational rearrangements of the channel protein, that yields high temperature sensitivity, the channels rely on a large change in the internal energy ($\Delta H$) to match and balance the energy associated with $T\Delta S$. The nice balance between $\Delta S$ and $\Delta H$ results in a small $\Delta G$ that can be easily overcome to activate the channel (Fig. S1). The balance between $\Delta H$ and $\Delta S$ determines the specific temperature range in which each thermoTRP channel operates. This can be characterized by the $T_{0.5}$ value, at which the temperature-

Author contributions: F.Y. and Y.C. performed research; F.Y., Y.C., and J.Z. analyzed data; K.W. and J.Z. designed research; and J.Z. wrote the paper.

The authors declare no conflict of interest.

*This Direct Submission article had a prearranged editor.

[1]To whom correspondence should be addressed. E-mail: jzheng@ucdavis.edu.

This article contains supporting information online at www.pnas.org/cgi/content/full/1000357107/DCSupplemental.

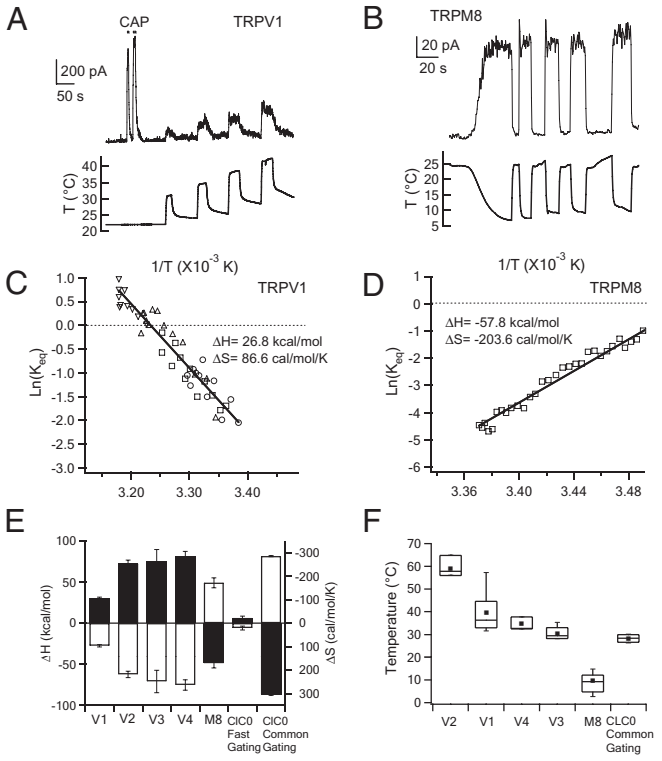


**Fig. 1.** Thermodynamic characterization of the temperature-dependent gating of thermoTRPs. (*A* and *B*) Inside-out patch recordings of temperature-driven activation of TRPV1 (*A*) or TRPM8 (*B*) expressed in HEK293 cells. Currents in response to 10 μM TRPV1 agonist capsaicin (CAP) seen in (*A*) confirm that they are mediated by TRPV1 channels. (*C* and *D*) Van't Hoff plots for the heat-elicited TRPV1 current (*C*) and cold-elicited TRPM8 current (*D*). The symbols in (*C*) represent current responses to four temperature jumps shown in *A*. Lines represent fits of the Van't Hoff equation, from which $\Delta H$ and $\Delta S$ are estimated. (*E*) Measured $\Delta H$ values (filled bars, left axis) and $\Delta S$ values (open bars, right axis) of thermoTRPs and CLC-0 channels. (*F*) Box-and-whisker plot of half-activation temperature $T_{0.5}$. The whisker top, box top, line inside the box, box bottom, and whisker bottom represent the maximum, 75th percentile, median, 25th percentile, and minimum value of each pool of $T_{0.5}$ measurements, respectively. Square dots indicate the average $T_{0.5}$ value. The data in *E* and *F* represent measurements from 3–14 patches.

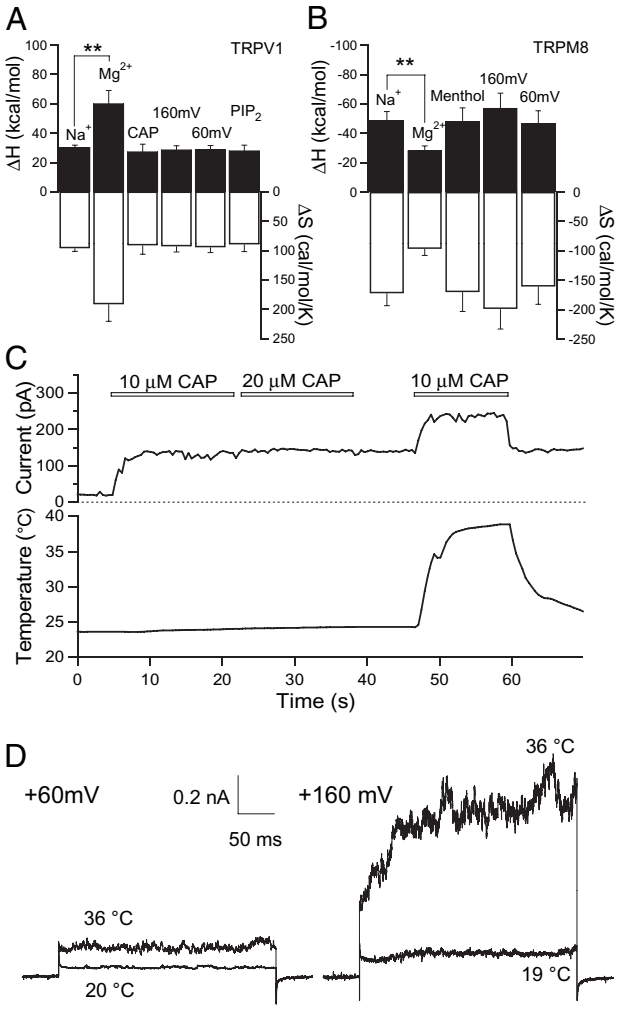


**Fig. 2.** Determination of a distinct temperature-sensitive activation pathway. (*A* and *B*) Changes in $\Delta H$ and $\Delta S$ of the temperature-driven activation measured under various conditions for TRPV1 (*A*) and TRPM8 (*B*). Filled bars represent $\Delta H$ values (left axis), and open bars correspond to $\Delta S$ values (right axis). **Significant difference at the level of $P < 0.01$. $n$ = 4–13 patches. (*C* and *D*) Representative inside-out patch recordings demonstrating additive effects of capsaicin (*C*) or voltage (*D*) on heat-induced TRPV1 activation. Leak currents are not subtracted.

dependent activation is 50% (Fig. 1*F*). Conceivably, the activation temperature of these thermosensors could be dynamically regulated through biological processes that affect $\Delta H$ and/or $\Delta S$.

**Activation of ThermoTRPs Involves Distinct Pathways.** Thermodynamic quantification allowed us to search for protein structures that convey high temperature sensitivity to thermoTRPs. Like many other TRP channels, thermoTRPs are polymodal receptors. It has been proposed that heat, voltage, and ligand activate thermoTRPs through a common mechanism in which heat and ligand interact with the voltage sensor and shift the voltage dependence of these channels (10). To test this hypothesis and identify the temperature-sensing structure, we monitored $\Delta H$ and $\Delta S$ while perturbing the channel with different physical and chemical stimuli. We found that although both strong depolarization and application of capsaicin could effectively activate TRPV1 at room temperature, the $\Delta H$ and $\Delta S$ of the temperature-dependent activation are not significantly affected by these stimuli (Fig. 2*A*). Whereas 1 μM capsaicin shifted the $T_{0.5}$ from 39 ± 3 °C ($n$ = 14) to 23 ± 2 °C ($n$ = 7), $\Delta H$ and $\Delta S$ for temperature-induced activation remained high [without capsaicin, $\Delta H$ = 29 ± 2 kcal/mol, $\Delta S$ = 94 ± 5 cal/mol/K ($n$ = 14); with 1 μM capsaicin, $\Delta H$ = 27 ± 3 kcal/mol, $\Delta S$ = 92 ± 11 cal/mol/K ($n$ = 7)]. A further increase in capsaicin concentration to 10 μM produced no detectable change ($\Delta H$ = 28 ± 5 kcal/mol, $\Delta S$ = 94 ± 7 cal/mol/K, $T_{0.5}$ = 21 ± 4 °C; $n$ = 3). PIP2, a potent TRPV1 modulator thought to bind to intracellular sites (16–19), also exhibited no obvious effect. Similarly, both depolarization and menthol failed to significantly change $\Delta H$ or $\Delta S$ in TRPM8 (Fig. 2*B*). These results indicate that although different stimuli can synergistically activate thermoTRPs, their actions involve different protein structures or pathways. Similar synergistic but structurally separate activation pathways are seen in the $Ca^{2+}$-activated voltage-dependent BK channels (20).

Evidence for a separate heat activation pathway in thermoTRPs was also provided by measuring the maximum current in the presence of combined stimuli. Activation of TRPV1 by capsaicin, for example, saturated at the low μM range. After full activation of TRPV1 by 10 μM capsaicin at room temperature, heat could still significantly increase the TRPV1 current beyond the maximum ligand-induced current level ($n$ = 9) (Fig. 2*C*). Similarly, voltage and temperature exhibited additive effects on TRPV1 activation ($n$ = 5) (Fig. 2*D*). These additive effects are

better explained by a mechanism in which driving forces from independent stimuli converge onto a common activation gate (21). They are not consistent with the common activation pathway hypothesis, which predicts a shift in the dynamic range but no change in the maximum activation level.

**ThermoTRP Channel Pores Are Involved in Temperature-Dependent Activation.** If temperature is sensed in thermoTRPs by a unique protein structure, where is the structure located? Hints come from thermodynamic measurements in which different permeant ions were compared. When monovalent permeant ions $K^+$ or $Na^+$ were replaced by divalent cations, such as $Mg^{2+}$, the $\Delta H$ and $\Delta S$ values measured from TRPV1 were doubled, whereas those measured from TRPM8 were substantially reduced (Fig. 2 *A* and *B*). This observation suggests that the large $\Delta S$-associated conformational rearrangement affects the interaction between permeant ions and the channel pore; that is, there is likely a substantial rearrangement of the pore conformation in response to temperature change. Whether movement in this part of the TRPV1 pore is also related to capsaicin-induced pore dilation remains to be determined (22).

Inspired by the permeant ion effects on thermodynamics and reports that pore mutations in TRPV1 and TRPV3 can selectively lock the temperature activation gate in the open or closed state (23, 24), we made a series of sequence replacements in the outer pore region of TRPV1. We found that replacing a 14-aa segment of the TRPV1 pore turret with an artificial sequence $G_4PG_4SG_4S$ (Fig. 3*A*) completely eliminated the channel's temperature response while leaving the capsaicin response intact (Fig. 3*B*). The mutant channels were properly assembled and trafficked (as judged by cell surface fluorescence from channel-tagged fluorescence proteins). Current recordings showed that the mutant channel exhibited a 25% increase in single-channel conductance compared with the WT channels (Fig. 3*C*), along with a slightly increased sensitivity to capsaicin (Fig. 3*D*). The conductance change is likely due to structural alternation of the channel pore, and the shift in capsaicin sensitivity might be due to mutational effects on the coupling of ligand binding to the activation gate. In contrast to the minor effects seen in ligand-induced activation, raising the temperature to above 40 °C ($T_{0.5}$ for TRPV1) failed to elicit a noticeable current from the mutant channels (Fig. 3*E*). We conclude that the absence of temperature-dependent current is due to a lack of temperature sensitivity in functional mutant channels.

**Movement of TRPV1 Pore Turret During Heat-Induced, but Not Ligand- or Voltage-Induced, Activation.** If the pore turret of thermoTRPs

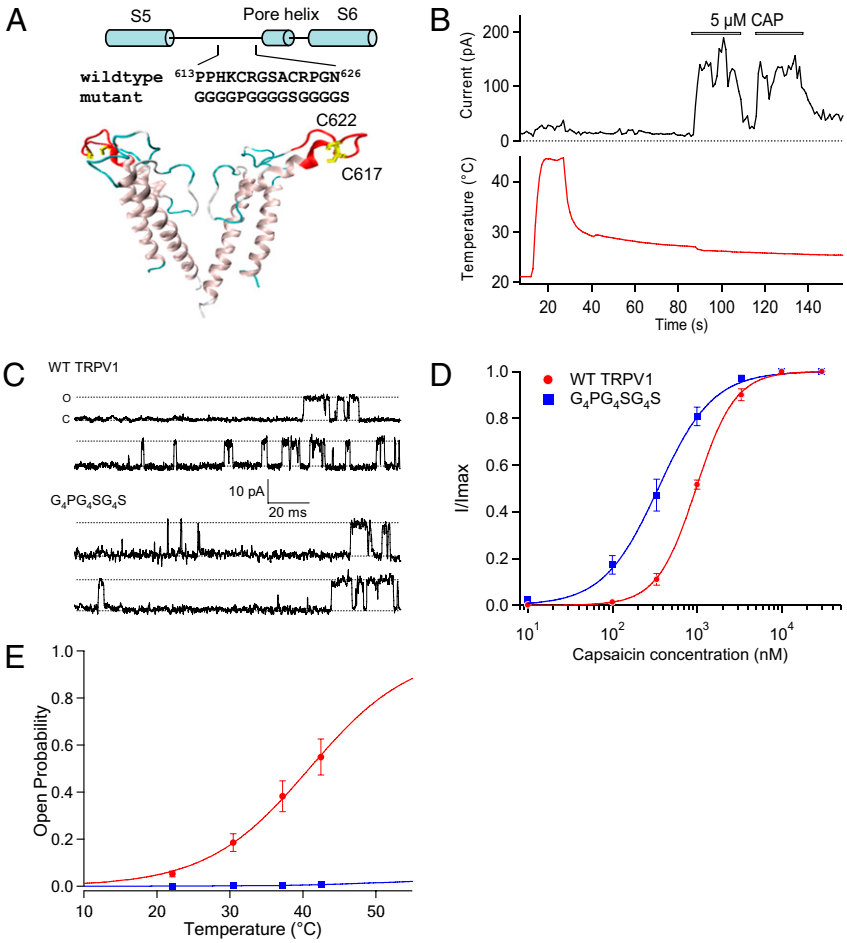


**Fig. 3.** Replacement of the pore turret sequence eliminates temperature-dependent gating. (*A*) A structural model of the channel pore showing the replaced turret sequence (in red) and the two cysteines, C617 and C622 (in yellow) used for fluorescence labeling. The structure is based on a model of the human TRPV1 (50). (*B*) Mutant channels containing the $G_4PG_4SG_4S$ sequence are insensitive to temperatures up to 45 °C but can be activated by capsaicin. A representative trace of 10 inside-out patches is shown; 2 other patches showed spontaneous channel activities at room temperature. (*C*) Representative single-channel traces recorded from inside-out patches at +80 mV. (*D*) Dose–response relationship for the WT and $G_4PG_4SG_4S$ mutant channels. Curves represent fits of a Hill equation. The $EC_{50}$ and Hill slope values are as follows: WT, 0.98 μM and 1.9 ($n$ = 3); mutant, 0.35 μM and 1.3 ($n$ = 5). (*E*) The relationship between open probability and temperature for the WT channels ($n$ = 12) and mutant channels ($n$ = 4).

participates in temperature sensing, then it would be expected to undergo conformational rearrangement in response to temperature changes. To directly monitor structural changes during temperature-dependent activation, we conducted site-directed fluorescence recordings (25). TRPV1 has two native cysteine residues in the pore turret sequence (Fig. 4*A*) that can be labeled by extracellularly applied sulfhydryl-reactive fluorophores (Fig. S2*A*). Mutations of these cysteines or modification with maleimide derivatives substantially altered $\Delta H$ and $\Delta S$, but did not remove temperature-sensitive gating (Fig. S2*B*). These observations are consistent with results from our sequence replacement experiment and suggest that these positions are indeed part of the structure involved in heat-induced conformational changes.

We attached fluorescein maleimide (FM) and tetramethylrhodamine maleimide (TMRM) to these cysteines and followed conformational changes with fluorescence resonance energy transfer (FRET) (Fig. 4*B*). Simultaneous recording of the time courses of current and fluorescence changes allowed us to directly correlate structural changes in the turret to channel activation (Fig. 4*C*). We observed substantial FRET increases during heat-induced TRPV1 activation in both WT channels (Fig. 4*C*) and mutant channels containing one of the two cysteines (Fig. 4*D*). These FRET increases suggest that TRPV1 turrets moved closer to each another during activation. Using a 50-Å characteristic distance *R0* (at which the FRET efficiency is 50%) (26), a single FM-TMRM pair separated by 44 Å (the modeled closed-state distance between C622 residues in neighboring subunits) needed to move 2–4 Å closer to yield an increase in FRET of the same magnitude as that observed in TRPV1. Background fluorescence recorded from cells expressing mutant channels missing both cysteines (cys-less) exhibited very low nonspecific FRET signals that were insensitive to temperature changes (Fig. 4*D*). Fluorophores attached to cysteines introduced individually at two extracellular S1-S2 linker positions (L461C and L467C) or at one S3-S4 linker position (K536C) in the cys-less background exhibited a positive FRET, but considerably lower than those from the pore turret, consistent with their expected peripheral locations and a distance between neighboring subunits much larger than $R_0$ (Fig. 4*D*). These channels could be effectively activated by heating; the FRET from these positions remained unchanged, however.

Additional FRET experiments indicated that the temperature-induced pore turret conformational change is independent of ligand- and voltage-induced TRPV1 activation. Channel activation induced by 10 μM capsaicin caused no change in FRET at the turret positions (Fig. 4*D*). Depolarization by 100 mV, from 60 mV to 160 mV, also failed to change the FRET at the turret positions and at the S3-S4 linker (Fig. 4*D*). These results suggest that activation of TRPV1 by capsaicin [which binds to the vicinity of the S2-S3 linker (27)] or voltage does not require significant conformational changes in the outer pore. The absence of a FRET change at the S3-S4 linker can be explained if the weak voltage dependence of TRPV1 originates not from transmembrane movement of the S3-S4 complex, which forms the voltage sensor in voltage-gated cation channels (28), but rather from transmembrane relocation of other charged structures. A less likely scenario is that the S3-S4 complexes in all subunits move vertically in response to voltage changes in a highly cooperative fashion (29). Taken together, our FRET results are consistent with the idea that heat is sensed in thermoTRPs with a protein structure distinct from those structures for sensing voltage and ligand stimuli (Fig. 4*E*).

## Discussion

We propose that heat, voltage, and ligand stimuli are sensed by thermoTRPs with different protein structures. Thermal energy

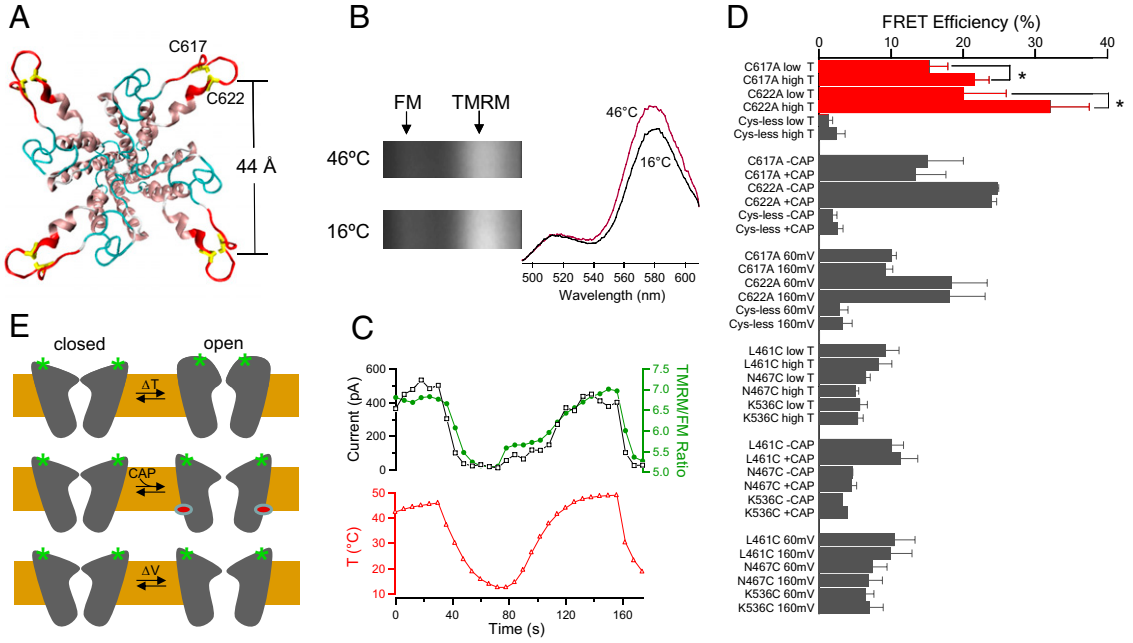


**Fig. 4.** Fluorescence recording of the temperature-induced structural changes in the TRPV1 pore turret. (*A*) Top view of the modeled TRPV1 pore structure, with the distance between $C_\beta$ of C622 of neighboring subunits labeled. (*B*) Spectral images of a cell expressing WT TRPV1 labeled with FM and TMRM at low and high temperatures. The corresponding spectra on the right are normalized by their FM peaks. (*C*) Simultaneous whole-cell current and fluorescence recordings from WT TRPV1 channels when the temperature is changed. (*D*) FRET efficiency measured from the outer pore positions as well as from two positions at the S1—S2 linker (L461C and N467C) and one position at the S3-S4 linker (K536C). "Low T" and "high T" indicate temperature below 25 °C and above 40 °C, respectively. Measurements with capsaicin (10 μM) and voltage were performed at room temperature. Cys-less indicates a mutant channel missing both C617 and C622. *$P < 0.05$. $n = 3$–5. (*E*) A schematic model of the proposed gating conformational changes in TRPV1 induced by heat, capsaicin, and voltage. Green stars represent fluorophores attached to the pore turret.

drives a reversible conformational change in the pore turret of heat-activated TRPV1 (and likely of cold-activated TRPM8 as well), which is coupled to the opening of the activation gate, S6 (30). Mutations in this region specifically affect the turret conformational changes through which they exert gating effects on temperature-dependent activation. The large amplitude of FRET changes indicates that the structural change in the pore is substantial, supporting the idea that the pore turret region is part of a "temperature sensor apparatus." Conformational changes in this region would be expected to cause significant changes in interactions among amino acids and/or between amino acids and the surrounding water/lipid molecules, giving rise to the large $\Delta H$ and $\Delta S$ that underlie high temperature sensitivity.

Recent studies have suggested that the outer pore region is involved in temperature gating of thermoTRPs. Random mutagenesis approaches have identified a number of mutations in the outer pore region that permanently lock the heat activation process in the activated or deactivated state (23, 24). It is possible that these mutations either disrupt the coupling of turret conformational changes to the activation gate or directly interfere with turret movement. Similarly, protonation of the outer pore sites may exert their gating effects by affecting turret movement (31). Studies based on point mutations and chimeras further suggest that heat-induced conformational change may involve channel structures beyond the pore region. In particular, the C-terminal intracellular region has been shown to affect temperature gating in a number of studies (18, 32–35). Furthermore, conformational changes in the turret may be coupled to movement in other parts of the thermoTRP channels, giving rise to the functional coupling observed among various stimuli (10, 36).

Identification of the pore turret as part of the temperature-sensing structure raises a number of interesting questions. What is the nature of structural changes in the turret? How does turret conformational change yield large $\Delta H$ and $\Delta S$? In the chloride channel CLC-0, the highly temperature-sensitive common gating is associated with a large conformational change in the intracellular C-terminal region (37). Here the subunit–subunit interaction is mediated mainly by hydrophobic interactions between cystathionine β-synthase tandem domains (38). Breaking these hydrophobic interactions would dramatically change both the internal energy ($\Delta H$) and the degrees of freedom ($\Delta S$) of the channel-environment system. The recently reported crystal structure of Kir2.2, which also contains a long outer pore sequence, shows a highly ordered turret structure (39). A better understanding of structural features of the thermoTRP turret will undoubtably help reveal the molecular mechanism of temperature sensing.

Identification of the thermoTRP turret as an important temperature-sensing structure may suggest intriguing pharmacologic approaches to specifically regulate cellular temperature responses. Whereas the majority of currently known ion channel inhibitors bind to and plug the ion permeation pore, inhibitors for inward rectifier potassium (Kir) channels, such as the bee venom toxin tertiapin (40), might selectively target the turret structures. Similarly, drugs developed following a similar strategy for thermoTRPs would be expected to have a much higher specificity than pore blockers, whose nondiscriminative effects on multiple channel types present serious risks for clinical use (41). For thermoTRPs, these types of drugs might have an additional advantage of being specific for heat-induced activation while sparing ligand and voltage regulation of the channel. The heat-insensitive gating behavior of functional turret mutants is consistent with this possibility.

## Methods

**Materials and Molecular Biology.** Murine thermoTRPs and CLC-0 cDNAs were fused with Cerulean or eYFP at the C terminus as described previously (37, 42). TRPV1 mutants were generated using the QuikChange II mutagenesis kit (Stratagene). Transfection of HEK293 cells followed standard protocols. Surface expression and functions of each fusion protein were assessed by fluorescence microscopy and patch-clamp recordings performed 1–2 days after transfection.

**Temperature Control.** Temperature control was achieved by perfusion of preheated or precooled solutions. Solutions were heated with an SHM-828 eight-line heater controlled by a CL-100 temperature controller (Harvard Apparatus). A custom-made manifold was attached to the output ports of the heater to deliver solutions to the recording chamber and provide heat insulation. Solutions were cooled by embedding the solution reservoirs in ice water and then perfused through a separate line. The patch pipette was placed about 1 mm from the solution output ports. A TA-29 miniature bead thermistor (Harvard Apparatus) was placed right next to the pipette to ensure accurate monitoring of local temperature. The thermistor's temperature readout was fed into an analog input of the patch amplifier and recorded simultaneously with current. With this method, we achieved rapid and reliable temperature changes between 7 °C and 55 °C. Full activation of TRPV2 required a higher temperature (43); as a result, TRPV2 measurements were performed with partially activated channels. The thermodynamic analysis was based on measurements of temperature-dependent changes in channel open probability, which were estimated from macroscopic currents after correction for temperature-dependent single-channel conductance (see below).

Thermodynamic measurement requires that the temperature-driven transition is at equilibrium state. In the present study, the rates of temperature-driven activation of all TRP channels except TRPV3 were faster than the maximum speed of temperature change that the setup could achieve. Thus, for these channels, solutions were first preheated to 50 °C or higher. The solution flow was then started to achieve a relatively high heating rate (Fig. S3). Although the rate of temperature increase with this approach was much slower than that seen in infrared laser–based heating approaches (44, 45) or the rapid solution-switching approach (46), it was sufficient to reach activation temperature in 1–2 seconds.

Because the temperature-driven activation of TRPV3 has a slow time course, for TRPV3 we first turned on the solution flow and then set the heater to the desired temperature. This way, the rate of temperature change was kept low (~0.15 °C/s) to ensure that the temperature-driven transition remained at equilibrium.

**Electrophysiology.** Patch-clamp recordings were done using an EPC10 amplifier (HEKA) driven by PatchMaster software (HEKA). The membrane potential was held at −80 mV, and currents were normally measured at +80 mV from inside-out patches. Both the pipette solution and the bath solution contained 130 mM NaCl, 0.2 mM EDTA, and 3 mM Hepes (pH 7.2). In some experiments, the 130 mM NaCl was replaced by 130 mM KCl, $MgCl_2$, or $BaCl_2$. Current signals were filtered at 2.9 kHz and sampled at 10 kHz. Single-channel amplitudes were measured at different temperatures from all-point histograms. The amplitude of leakage current was measured after the $Ba^{2+}$-containing solution was applied to block TRP channel currents measured from inside-out patches (Fig. S4).

**Calculation of ΔH and ΔS.** To calculate the enthalpic change, $\Delta H$, and entropic change, $\Delta S$, of the temperature-driven transition, we constructed Van't Hoff plots and fitted them to the equation $\ln K_{eq} = -\frac{\Delta H}{RT} + \frac{\Delta S}{R}$, where $K_{eq}$ is the equilibrium constant calculated from the channel open probability, $R$ is the gas constant, and $T$ is temperature. The following steps were taken to measure the open probability at different temperatures. First, the temperature dependence of single-channel conductance was determined for each thermoTRP channel type with each conducting ion type (Fig. S5). Macroscopic currents were corrected for changes in single-channel conductance by converting them to a level as if the temperature were 20 °C. The average current amplitude and the corresponding variance were estimated from the plateau phase of each sweep. Noise analysis was then applied to estimate the number of channels and the maximum current level (47). The open probability was calculated as the ratio between the corrected macroscopic current and the maximum current calculated by the noise analysis.

**Site-Directed Fluorescence Recordings and FRET Quantification.** For fluorescence recordings, TMRM (Invitrogen) and FM (Toronto Research Chemicals) were covalently linked to either extracellular cysteine C617 or C622 of TRPV1, with the other mutated to an alanine, or to cysteines introduced into the TRPV1 channel background in which both C617 and C622 had been mutated to alanines. The time course of fluorophore attachment was monitored by patch clamping (Fig. S2A). In brief, after a whole-cell patch was formed, a mixture of FM and TMRM at a concentration ratio of 1:1

was perfused onto the cell, and the change in current amplitude due to attachment of fluorophores to the cysteine residues was monitored. Free fluorophores were washed out of the bath solution after fluorescence labeling was complete and the current amplitude reached a stable level.

The imaging system was built on a Nikon TE2000-U microscope. The excitation light was generated by an Ar laser. The duration of light exposure was controlled by a computer-driven mechanical shutter (Uniblitz). A 40× oil-immersion objective (NA 1.30) was used in these experiments. Spectral measurements were performed with an Acton SpectraPro 2150i spectrograph in conjunction with a Roper Cascade 128B CCD camera. Both the shutter and the camera were controlled by MetaMorph software (Universal Imaging), synchronized with PatchMaster. In this way, the current and the spectral image were recorded simultaneously. From the spectral image, the TMRM/FM intensity ratio was calculated and used to follow the dynamic gating conformational changes during gating. To compare conformational changes at different channel positions under various experimental conditions, FRET efficiency was calculated from the increase in TMRM emission due to energy transfer. TMRM emission was separated from FM emission by fitting of standard spectra. After the direct excitation component of the TMRM emission was removed, the FRET efficiency value was calculated as described previously (48).

In the spectra FRET mode, two filter cubes (Chroma) were used. Cube I contained Z488/20 (excitation), z488rdc (dichroic), and HQ500lp (emission), and cube II contained Z514/10, z514rdc, and HQ530lp. Two spectroscopic images were obtained from each cell, one with the FM excitation at 488 nm using cube I and the other with the TMRM excitation at 514 nm using cube II. From these two images, the total emission spectrum and the TMRM emission spectrum, respectively, were constructed. Standard emission spectra also were collected from cells labeled with only TMRM or FM and used to separate cross-contamination between FM and TMRM due to spectra overlaps (49).

The analysis of temperature-dependent fluorescence changes due to channel gating had to take into account the fact that fluorescence emission itself is also temperature-sensitive. To correct for the intrinsic temperature dependence of FM and TMRM, the temperature sensitivity of these fluorophores was determined by measuring the fluorescence intensity at varying temperatures (Fig. S6). Before any quantitative analyses were carried out, all fluorescence recordings were corrected by converting the fluorescence intensity to that expected at 23 °C.

**ACKNOWLEDGMENTS.** We thank Dr. Fred Sigworth for commenting on the manuscript; Dr. Antonio Ferrer-Montiel for sharing the human TRPV1 pore structure model; Drs. Tsung-Yu Chen, Veit Flockerzi, Sharona Gordon, Itaru Kojima, Ardem Patapoutian, David Piston, Roger Tsien, Ulrich Wissenbach, and Michael Zhu for providing constructs; and members of the Zheng laboratory for providing assistance. This work was supported by grants from the National Institutes of Health (REY016754A) and American Heart Association (0665201Y), a UC Davis Health System Research Award (to J.Z.), and grants from the National Science Foundation of China (30970919) and Ministry of Education of China 111 Project (B07001) (to K.W.W.).

1. Clapham DE (2003) TRP channels as cellular sensors. *Nature* 426:517–524.
2. Jordt SE, McKemy DD, Julius D (2003) Lessons from peppers and peppermint: The molecular logic of thermosensation. *Curr Opin Neurobiol* 13:487–492.
3. Dhaka A, Viswanath V, Patapoutian A (2006) TRP ion channels and temperature sensation. *Annu Rev Neurosci* 29:135–161.
4. Venkatachalam K, Montell C (2007) TRP channels. *Annu Rev Biochem* 76:387–417.
5. Arenkiel BR, Klein ME, Davison IG, Katz LC, Ehlers MD (2008) Genetic control of neuronal activity in mice conditionally expressing TRPV1. *Nat Methods* 5:299–302.
6. Huang SM, et al. (2008) Overexpressed transient receptor potential vanilloid 3 ion channels in skin keratinocytes modulate pain sensitivity via prostaglandin E2. *J Neurosci* 28:13727–13737.
7. Mandadi S, et al. (2009) TRPV3 in keratinocytes transmits temperature information to sensory neurons via ATP. *Pflugers Arch* 458:1093–1102.
8. Doyle DA, et al. (1998) The structure of the potassium channel: Molecular basis of $K^+$ conduction and selectivity. *Science* 280:69–77.
9. Long SB, Campbell EB, Mackinnon R (2005) Crystal structure of a mammalian voltage-dependent Shaker family $K^+$ channel. *Science* 309:897–903.
10. Voets T, et al. (2004) The principle of temperature-dependent gating in cold- and heat-sensitive TRP channels. *Nature* 430:748–754.
11. Voets T, Owsianik G, Janssens A, Talavera K, Nilius B (2007) TRPM8 voltage sensor mutants reveal a mechanism for integrating thermal and chemical stimuli. *Nat Chem Biol* 3:174–182.
12. Brauchi S, Orio P, Latorre R (2004) Clues to understanding cold sensation: Thermodynamics and electrophysiological analysis of the cold receptor TRPM8. *Proc Natl Acad Sci USA* 101:15494–15499.
13. Imai K, Yonetani T (1975) Thermodynamical studies of oxygen equilibrium of hemoglobin: Nonuniform heats and entropy changes for the individual oxygenation steps and enthalpy-entropy compensation. *J Biol Chem* 250:7093–7098.
14. Liu B, Hui K, Qin F (2003) Thermodynamics of heat activation of single capsaicin ion channels VR1. *Biophys J* 85:2988–3006.
15. Pusch M, Ludewig U, Jentsch TJ (1997) Temperature dependence of fast and slow gating relaxations of ClC-0 chloride channels. *J Gen Physiol* 109:105–116.
16. Prescott ED, Julius D (2003) A modular PIP2 binding site as a determinant of capsaicin receptor sensitivity. *Science* 300:1284–1288.
17. Klein RM, Ufret-Vincenty CA, Hua L, Gordon SE (2008) Determinants of molecular specificity in phosphoinositide regulation: Phosphatidylinositol (4,5)-bisphosphate (PI (4,5)P2) is the endogenous lipid regulating TRPV1. *J Biol Chem* 283:26208–26216.
18. Brauchi S, et al. (2007) Dissection of the components for PIP2 activation and thermosensation in TRP channels. *Proc Natl Acad Sci USA* 104:10246–10251.
19. Lukacs V, et al. (2007) Dual regulation of TRPV1 by phosphoinositides. *J Neurosci* 27: 7070–7080.
20. Horrigan FT, Aldrich RW (2002) Coupling between voltage sensor activation, $Ca2^+$ binding and channel opening in large conductance (BK) potassium channels. *J Gen Physiol* 120:267–305.
21. Matta JA, Ahern GP (2007) Voltage is a partial activator of rat thermosensitive TRP channels. *J Physiol* 585:469–482.
22. Chung MK, Güler AD, Caterina MJ (2008) TRPV1 shows dynamic ionic selectivity during agonist stimulation. *Nat Neurosci* 11:555–564.
23. Myers BR, Bohlen CJ, Julius D (2008) A yeast genetic screen reveals a critical role for the pore helix domain in TRP channel gating. *Neuron* 58:362–373.
24. Grandl J, et al. (2008) Pore region of TRPV3 ion channel is specifically required for heat activation. *Nat Neurosci* 11:1007–1013.
25. Zheng J, Zagotta WN (2000) Gating rearrangements in cyclic nucleotide-gated channels revealed by patch-clamp fluorometry. *Neuron* 28:369–374.
26. Wu P, Brand L (1994) Resonance energy transfer: Methods and applications. *Anal Biochem* 218:1–13.
27. Jordt SE, Julius D (2002) Molecular basis for species-specific sensitivity to "hot" chili peppers. *Cell* 108:421–430.
28. Jiang Y, et al. (2003) X-ray structure of a voltage-dependent $K^+$ channel. *Nature* 423: 33–41.
29. Cha A, Snyder GE, Selvin PR, Bezanilla F (1999) Atomic scale movement of the voltage-sensing region in a potassium channel measured via spectroscopy. *Nature* 402: 809–813.
30. Salazar H, et al. (2009) Structural determinants of gating in the TRPV1 channel. *Nat Struct Mol Biol* 16:704–710.
31. Jordt SE, Tominaga M, Julius D (2000) Acid potentiation of the capsaicin receptor determined by a key extracellular site. *Proc Natl Acad Sci USA* 97:8134–8139.
32. Brauchi S, Orta G, Salazar M, Rosenmann E, Latorre R (2006) A hot-sensing cold receptor: C-terminal domain determines thermosensation in transient receptor potential channels. *J Neurosci* 26:4835–4840.
33. Vlachová V, et al. (2003) Functional role of C-terminal cytoplasmic tail of rat vanilloid receptor 1. *J Neurosci* 23:1340–1350.
34. Valente P, et al. (2008) Identification of molecular determinants of channel gating in the transient receptor potential box of vanilloid receptor I. *FASEB J* 22:3298–3309.
35. García-Sanz N, et al. (2007) A role of the transient receptor potential domain of vanilloid receptor I in channel gating. *J Neurosci* 27:11641–11650.
36. Tominaga M, et al. (1998) The cloned capsaicin receptor integrates multiple pain-producing stimuli. *Neuron* 21:531–543.
37. Bykova EA, Zhang XD, Chen TY, Zheng J (2006) Large movement in the C terminus of CLC-0 chloride channel during slow gating. *Nat Struct Mol Biol* 13:1115–1119.
38. Ignoul S, Eggermont J (2005) CBS domains: Structure, function, and pathology in human proteins. *Am J Physiol Cell Physiol* 289:C1369–C1378.
39. Tao X, Avalos JL, Chen J, MacKinnon R (2009) Crystal structure of the eukaryotic strong inward-rectifier $K^+$ channel Kir2.2 at 3.1-A resolution. *Science* 326:1668–1674.
40. Jin W, Lu Z (1998) A novel high-affinity inhibitor for inward-rectifier $K^+$ channels. *Biochemistry* 37:13291–13299.
41. Sanguinetti MC, Tristani-Firouzi M (2006) hERG potassium channels and cardiac arrhythmia. *Nature* 440:463–469.
42. Cheng W, Yang F, Takanishi CL, Zheng J (2007) Thermosensitive TRPV channel subunits coassemble into heteromeric channels with intermediate conductance and gating properties. *J Gen Physiol* 129:191–207.
43. Caterina MJ, Rosen TA, Tominaga M, Brake AJ, Julius D (1999) A capsaicin-receptor homologue with a high threshold for noxious heat. *Nature* 398:436–441.
44. Liang S, et al. (2009) Temperature-dependent activation of neurons by continuous near-infrared laser. *Cell Biochem Biophys* 53:33–42.
45. Yao J, Liu B, Qin F (2009) Rapid temperature jump by infrared diode laser irradiation for patch-clamp studies. *Biophys J* 96:3611–3619.
46. Kuno M, et al. (2009) Temperature dependence of proton permeation through a voltage-gated proton channel. *J Gen Physiol* 134:191–205.
47. Sigworth FJ (1980) The variance of sodium current fluctuations at the node of Ranvier. *J Physiol* 307:97–129.
48. Zheng J, Trudeau MC, Zagotta WN (2002) Rod cyclic nucleotide-gated channels have a stoichiometry of three CNGA1 subunits and one CNGB1 subunit. *Neuron* 36:891–896.
49. Takanishi CL, Bykova EA, Cheng W, Zheng J (2006) GFP-based FRET analysis in live cells. *Brain Res* 1091:132–139.
50. Fernández-Ballester G, Ferrer-Montiel A (2008) Molecular modeling of the full-length human TRPV1 channel in closed and desensitized states. *J Membr Biol* 223:161–172.